**International Journal of Electrical and Computer Engineering (IJECE)**
Vol. 11, No. 4, August 2021, pp. 2842~2855
ISSN: 2088-8708, DOI: 10.11591/ijece.v11i4.pp2842-2855 

# Adaptive backstepping control of induction motor powered by photovoltaic generator

**M. Madark, A. Ba-razzouk, E. Abdelmounim, M. El Malah**
System Analysis and Information Processing Team, Mathematics, Informatics and Engineering Sciences Laboratory, Science and Technical Faculty, Hassan First University, Settat, Morocco

**Article Info**

***Article history:***

Received Jul 20, 2020
Revised Oct 17, 2020
Accepted Dec 5, 2020

***Keywords:***

Adaptive control
Backstepping control
Centrifugal pump
Induction motor
Nonlinear MPPT

**ABSTRACT**

This paper is aimed at addressing the design of an effective adaptive nonlinear control of a photovoltaic (PV) water pumping system powering a submersible induction motor and a centrifugal water pump. Four objectives are achieved using an adaptive Backstepping controller. First, it is applied to ensure maximum power point tracking, and uses the latter as a reference in regulation of the rotor speed to convert the maximum electrical power into maximum mechanical power. Second, the adaptive controller is synthesized to control motor rotor flux and restrict the magnetic circuit to its linear interval. Third, it is used to online estimate the rotor time-constant and the load torque disturbance estimation. Finally, this controller is employed to limit the stator currents to protect induction motor windings. Mathematical modelling of the main elements of the system is presented. A sliding mode rotor flux estimator is employed in the output feedback control of the whole system. DC-AC converter is controlled by pulse width modulation. The feasibility, the robustness and the effectiveness of the proposed adaptive nonlinear controller are evaluated through simulations in MATLAB/Simulink environment.



***Corresponding Author:***

Mhamed Madark
Department of Applied Physics, Science and Technical Faculty
Hassan First University
Settat, Morocco
Email: m.madark1987@gmail.com

## 1. INTRODUCTION

Renewable energies continue to gain popularity around the world, consolidating their dominance over fossil fuels in terms of new installed electricity production capacities. The use of coal, for its part, is continuing to decline worldwide. In 2019, renewable energies represented 72% of new installations in practically all regions, except in Africa and the Middle East, where their respective shares are 52% and 26%. These additions brought the share of renewable energy in total global electricity production capacity to 34.7%, compared to 33.3% at the end of 2018 [1].

The development of renewable energies is arousing a huge interest in the Moroccan national energy strategy. The latter is moving towards the diversification of energy supply sources by increasing the contribution of green energies to 42% of total installed electrical power by 2020. Energy efficiency, alongside the development of renewable energies, is a priority in the national energy strategy. The goal of this program is to save 12% of energy consumption in 2020 and 15% in 2030 [2].

The photovoltaic system is one of the most widely used renewable energy sources. One of its main applications is the direct solar photovoltaic water pumping system. This is due to its simplicity, maintenance free and its ability of operating without storage batteries. The system consists of a PV generator, a pumping

control scheme, a sensor system, a centrifugal pump and an electrical motor drive. The advantage of direct system is the correspondence of the radiation curve with the water demand curve [3]. It also makes it possible to extract water in rural areas, where the cost of installing a conventional grid line is expensive.

The energy supplied by the photovoltaic generator remains expensive despite the lowering of the cost of the watt-peak. It is therefore necessary to operate these generators at their maximum power point (MPP). To tackle this problem, an approach consists in adding a static converter between the generator and the load to extract the optimal power. Many maximum power point tracking (MPPT) algorithms have been proposed in the literature to control a DC-DC converter placed between the PV generator and the load. The goal of this algorithm is to maximize the power extraction from the solar panels, and thus increase the efficiency of the system. Perturbation and observation (P&O) technique is the most widely used due to its simplicity and low cost of implementation. Despite these advantages, this algorithm may present poor performance during rapid changes in climatic conditions [4]. More efficient techniques based on the measurement of power such as "Increment of conductance" and "Hill Climbing" are proposed in the literature [5, 6]. However, controllers constitute promising solutions to counterbalance the shortcomings of conventional schemes [7, 8]. Furthermore, Fuzzy Logic and Artificial Neural Networks are more efficient, but their implementation is more complicated [9]. In [10], a comparative study of three controllers applied to solar photovoltaic water pumping system using the indirect rotor flux oriented control (IRFOC) is presented. A robust integral Backstepping control design to track the MPP of a photovoltaic pumping system was proposed in [11].

The solar pumping system exists in several topologies. The use of induction motors (IM) increases the mechanical robustness, reliability and the operation of high-efficiency of the system [12, 13]. This machine has low manufacturing costs and its ability to accept a wide range of voltage. However, IM control remains complex due to its state model nonlinearity, its very high degree, parameters variations especially the rotor time-constant and the coupling between flux and electromagnetic torque. Therefore, IRFOC cannot decouple these two variables. In an IRFOC, rotor time-constant is the main parameter responsible for performance deterioration. In order to maintain dynamic performance of IRFOC combined with the nonlinear controller, this parameter must be estimated and adapted. In literature, many proposed nonlinear controllers for solar photovoltaic water pumping system do not focus on parameters variations of IM. Moreover, the validation of most of the induction motor rotor time-constant estimators in literature assumed that the DC-link voltage and the load torque disturbance are constants, and the modelling of this load torque was considered proportional to the square of the rotor speed. These assumptions cannot validate the proposed research works on adaptive laws. Therefore, it is necessary to develop a new rotor time-constant estimator based on quadrature component of the rotor flux and use it in the solar photovoltaic water pumping system. In this system, load torque disturbance estimator of centrifugal pump depends on rotor time constant and has to be estimated and adapted. Consequently, in [14], a vector control of IM drive powered by photovoltaic (PV) arrays using a current control voltage source inverter is presented. Backstepping control of centrifugal water pump driven by an IM was proposed in [15] with the aim to operate the PV generator at MPP using variable-step P&O. In [16], a three-phase IM using sliding-mode control (SMC) was presented. In all these works, their authors did not address the issue of rotor time-constant variations.

In this paper, the proposed system employs a centrifugal water pump. To establish the control of the induction motor, it is necessary to model this pump. Pump theory can be used to generate a theoretical correlation "Head-Flow" characteristics, and "Efficiency-Flow". However, due to complex phenomena during operations, such theoretical characteristics at a reference speed cannot reflect reality [17]. Therefore, the "Head-Flow" and "Efficiency-Flow" curves must be obtained by experimental measurements. Once the measurements of "Head-Flow" characteristics and "Efficiency-Flow" are known, a polynomial function can be used to generate these correlations. To generate the "Head-Flow" characteristics, [17] a third order polynomial is used. Fam and Goswami [18] used a second order polynomial characteristic. In [19] a second order polynomial characteristic with elimination of the linear term is proposed. In the literature many research works proposed a square load model of the centrifugal pump [14, 20-22]. Control laws require the knowledge of load torque. In fact, the measurement entails vibrations and can cause instability of the system. Moreover, developing mathematical modelling of centrifugal pump is a real and a complex issue. With the aim to solve the drawbacks of mechanical sensors and to avoid the use of centrifugal pump mathematical model (torque proportional to square of the speed) in control laws, an observer of load torque disturbance will be proposed. This observer only requires the measurable outputs of the induction motor.

This paper organized in five sections describing the modelling and the proposed control approach of a solar photovoltaic water pumping system. In the section 2, mathematical modelling of PV generator and its characteristics, DC-DC boost converter, DC-AC converter, induction motor and centrifugal pump and its characteristics are presented. Nonlinear MPPT, inverter control law, rotor time-constant and load torque observers are given in section 3. In section 4 simulation results are presented and discussed. Conclusions and perspectives are given in section 5.

## 2. MODELLING OF THE SYSTEM

Solar photovoltaic water pumping system consists at least of the following elements: PV generator, induction motor, centrifugal water pump, controller, storage tank, DC link, rotor speed sensor.

### 2.1. Mathematical model of the PV generator

PV cells are generally associated in series and in parallel, and then encapsulated to form a photovoltaic module. Figure 1 illustrates the electrical equivalent circuit of a PV cell. PV generator is made up of interconnection of several modules to respond to the required power. PV modules are usually connected in series-parallel to increase the voltage and current at the generator output. Therefore, PV generator model is deduced from that the PV cell. Equations (1)-(3) describe the PV cell model.

$$I_{cell} = I_{ph} - I_s\left(\exp\left(q\frac{V_{cell} + R_{ss}I_{cell}}{\gamma KT}\right) - 1\right) - \frac{V_{cell} + R_{ss}I_{cell}}{R_{sh}} \quad (1)$$

$$I_{ph} = \frac{E}{E_{ref}}\left(I_{sc} + K_i\left(T - T_r\right)\right) \quad (2)$$

$$I_s = I_{rs}\left(\frac{T}{T_r}\right)^3 \exp\left(-\frac{qE_{g0}}{\gamma K}\left(\frac{1}{T} - \frac{1}{T_r}\right)\right) \quad (3)$$

where $I_{cell}$ , $V_{cell}$ , $I_{ph}$ , $I_{rs}$ , $I_{sc}$ , $E_{ref}$, $E$, $T_r$, $T$, $K_i$, $q$, $K$, $R_{ss}$ and $R_{sh}$ are the current across the cell, the solar cell output voltage, photo-current, reverse saturation current, cell short-circuits current at 298 °K and 1 kW/m², reference solar irradiation in W/m$^2$, solar irradiation in W/m$^2$, cell's reference temperature, temperature on absolute scale, cell's short-circuit its current temperature coefficient, electron charge, Boltzmann's constant, and intrinsic series and parallel resistors of the cell respectively. Current and voltage outputs of the PV generator are deduced from those of the PV cell.

$$I_{pv} = N_p I_{cell} \ , \ V_{pv} = N_s V_{cell} \quad (4)$$

with $N_p$ and $N_s$ being parallel and series wired PV solar panels respectively. With the aim to plot the nonlinear P-V characteristics of the PV generator and to define MPP under different atmospheric conditions, electrical specifications of the SM55 PV panel and MATLAB/Simulink environment are employed and given in Table 1.

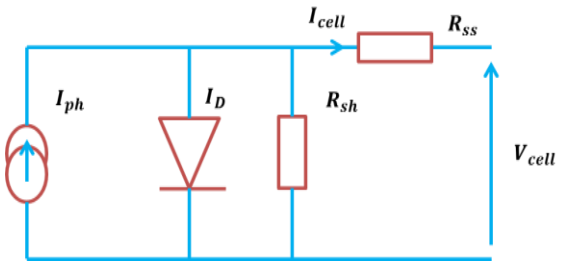


Figure 1. Electrical schems of PV cell

Table 1. Electrical specifications of SM55 PV panel

| Electrical specifications | Rating Values |
|---|---|
| Maximum power rating $Pe_{max}$ (W) | 55 |
| Rated current at the MPP (A) | 3.15 |
| Rated voltage at the MPP (V) | 17.4 |
| Short circuit current $I_{sc}$ (A) | 3.45 |
| Open circuit voltage $V_{oc}$ (V) | 21.7 |
| Curent temperature coefficient (mA/°C) | 1.2 |
| $n_s$ solar cells connected in series | 36 |
| $n_p$ solar cells connected in parallel | 1 |

Adaptive nonlinear Backstepping controller must track these trajectories. MPP coordinates are recapitulated in Table 2 and used to validate the proposed controller. Figure 2 presents the P-V characteristic of PV generator under study. This generator is made up from 4 parallel chains, and each one is composed of 23 series SM55 PV panels.

Table 2. MPP coordinates of the PV generator

| Coordinates of MPP | T (°K) | E(W/m$^2$) | $V_{mpp}$ (V) | $P_{mpp}$ (W) | $I_{mpp}$ (V) |
|---|---|---|---|---|---|
| MPP1 | 298.15 | 1000 | 395.80 | 5007.00 | 12.65 |
| MPP2 | 298.15 | 500 | 372.80 | 2346.00 | 6.29 |
| MPP3 | 323.15 | 500 | 326.90 | 2032.00 | 6.21 |

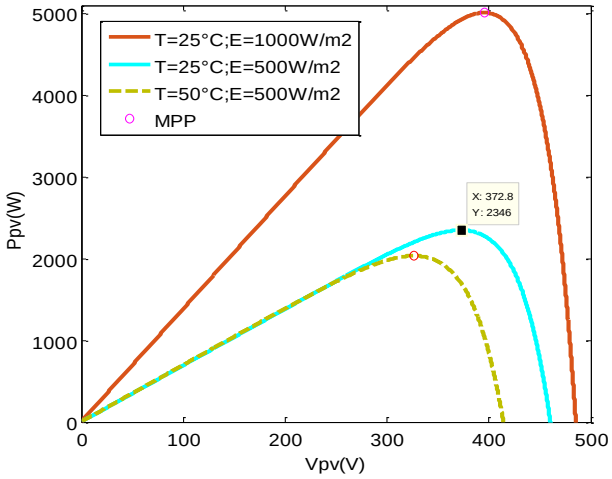


Figure 2. P-V characteristic of PV generator

### 2.2. Mathematical model of the DC-DC converter

This converter is used to boost PV generator voltage, to reduce the PV panels number used and to track the MPP. The boost converter state space representation is given as (5).

$$\begin{cases} \dfrac{dV_{pv}}{dt} = \dfrac{I_{pv} - I_L}{C_p} \\ \dfrac{dI_L}{dt} = \dfrac{V_{pv} - (1-u)V_b}{L_b} \\ \dfrac{dV_b}{dt} = \dfrac{(1-u)I_L - I_b}{C_b} \end{cases} \tag{5}$$

with $V_{pv}$, $V_b$, $C_p$, $C_b$, $u$, $I_{pv}$, $I_b$, $I_L$ and $L_b$ being input voltage, output voltage, input capacitor, output capacitor, duty cycle, input inductance, output current, inductance current and output inductance respectively.

### 2.3. Mathematical model of the DC-AC converter

IM is supplied through a three-phase current controlled voltage source inverter (CC-VSI). This inverter is modeled using the relationship between the switching functions, the outputs voltages $[V_{AN} \quad V_{BN} \quad V_{CN}]^T$ and the DC-link voltages [23-25].

$$\begin{bmatrix} V_{AN} \\ V_{BN} \\ V_{CN} \end{bmatrix} = \frac{1}{3}\begin{bmatrix} 2 & -1 & -1 \\ -1 & 2 & -1 \\ -1 & -1 & 2 \end{bmatrix}\begin{bmatrix} K_1 \\ K_2 \\ K_3 \end{bmatrix} V_b \tag{6}$$

with $K_1$, $K_2$, $K_3$ and $V_b$ being the switching functions and DC-link voltage respectively.

### 2.4. Mathematical model of the induction motor

IM is supplied through a three-phase current controlled voltage source inverter (CC-VSI). This inverter is modeled using the relationship between the switching functions, the outputs and the DC-link voltages:

$$\frac{d}{dt}\begin{bmatrix}\omega_r\\ \Psi_{rd}\end{bmatrix}=\begin{bmatrix}-a_2-a_3\omega_r\\ a_5\Psi_{rd}\end{bmatrix}+\begin{bmatrix}0 & a_1\Psi_{rd}\\ a_4 & 0\end{bmatrix}\begin{bmatrix}I_{sd}\\ I_{sq}\end{bmatrix} \tag{7}$$

with $\omega_r$, $\Psi_{rd}$, $I_{sd}$ and $I_{sq}$ being the rotor speed, rotor flux direct component and stator current components respectively. IM parameters J, p, M, F, $L_r$, $T_L$ and $\tau_r$ are respectively moment of inertia, poles pair number, mutual inductance, coefficient of friction, rotor inductance, load torque and rotor time-constant and $a_i$ coefficients are defined as (8).

$$a_1=\frac{3}{2}\frac{p^2M}{JL_r};\quad a_2=\frac{pT_L}{J};\quad a_3=\frac{pF}{J};\quad a_4=\frac{M}{\tau_r};\quad a_5=-\frac{1}{\tau_r} \tag{8}$$

### 2.5. Mathematical model of the centrifugal pump

To extrapolate the "Head-Flow" characteristics of the pump corresponding to a different reference speed $\omega_r^{'}$, the affinity laws can be used [10, 19]. The current values of the flow $q^{'}$, the head $h^{'}$ and the pressure $p_r'$ can be expressed as a function of the reference values of the flow $q$, the head $h$ and the pressure $p_r$:

$$q^{'}=q\left(\frac{\omega_r^{'}}{\omega_r}\right);\quad h^{'}=h\left(\frac{\omega_r^{'}}{\omega_r}\right)^2\quad p_r{}^{'}=p_r\left(\frac{\omega_r^{'}}{\omega_r}\right)^2 \tag{9}$$

Based on the centrifugal pump experimental data listed in the manufacturer's catalog, it is possible to choose the polynomial approximation, which is derived from the equation of the Euler pulse moment [26-27], to determine the "Head-Flow" characteristics of the pump. The pressure can be expressed by (10).

$$p_r=\rho gh=\rho\left(k(c_0-c_1q)-c_2q^2-c_3(q-q_d)^2\right) \tag{10}$$

with $\rho$, $k$, $c_i$, g, and $q_d$ being the density of the fluid, the correction factor, the approximation coefficients, the gravity acceleration and the nominal delivery of the pump respectively. Mechanical power is given as (11):

$$P_m'=C_r'\omega_r^{'}=\frac{P_h'}{\eta}=\frac{\rho gh'q'}{\eta} \tag{11}$$

with $\eta$ being the efficiency of the IM and the pump. Assuming that the efficiency remains constant when the speed varies, we can consider in this case that the centrifugal pump applies a load torque proportional to the square of the rotor speed. Therefore, the pump load torque is expressed as (12):

$$C_r'=K\omega_r'^2 \tag{12}$$

where:

$$K=\frac{\rho hq}{\eta\omega_r^3} \tag{13}$$

The total dynamic head (TDH) is composed of the static and dynamic head and is given (14).

$$h_t=h_s+h_d \tag{14}$$

White [28] showed that the $h_d$ can be related to the flow and the pipeline system parameters (15).

$$h_d = \frac{flq^2}{2gdS^2} \tag{15}$$

with *f, l, d, q, S* and g being respectively the Darcy friction coefficient, the pipeline length, the pipeline diameter, the fluid flow, the section area and the gravity acceleration. There are other models of simplified hydraulic systems [19] adopted the (16).

$$h_p = h_s + kq^2 \tag{16}$$

With *k* being a constant to be designed using the centrifugal pump data. We will consider a centrifugal pump that delivers 20 $m^3/h$ to a water tank with a total dynamic head of 33.57 m and a power of 5.5 kW. The Grundfos NBG 65-40-315/334 pump, which uses the Grundfos performance curves, shown in Figure 3, is chosen. This pump is intended for drinking water supply and is equipped with a 5.5 kW 132SA type motor. At speeds other than the reference speed (1460 rpm) and using (10), the process of determining these four constants requires measurements of the pump head at a minimum of four flow rates. Based on the "Head-Flow" characteristics shown in Figure 3, these four parameters define the centrifugal pump model by the polynomial approximation in Simscape. The block diagram in Simscape is given in Figure 4. Figure 5 shows the pump and the pipeline "Head-Flow" characteristics. The use of the pump Simscape block requires the determination of the approximation coefficients $c_0$, $c_1$, $c_2$ and $c_3$. These coefficients are given (17).

$$\begin{bmatrix} c_0 \\ c_1 \\ c_2 \\ c_3 \end{bmatrix} = \begin{bmatrix} k & -kq_1 & -q_1^2 & -(q_1-q_d)^2 \\ k & -kq_2 & -q_2^2 & -(q_2-q_d)^2 \\ k & -kq_3 & -q_3^2 & -(q_3-q_d)^2 \\ k & -kq_4 & -q_4^2 & -(q_4-q_d)^2 \end{bmatrix}^{-1} \begin{bmatrix} gh_1 \\ gh_2 \\ gh_3 \\ gh_4 \end{bmatrix} \tag{17}$$

The "Load torque-rotor speed" characteristic is reported in Figure 6. According to Figure 6, "Load torque-Rotor speed" characteristic of the centrifugal pump is highly nonlinear. This characteristic can be similar to that given in (12) in particular conditions. One of these conditions is to assume that the efficiency of the pump is constant.

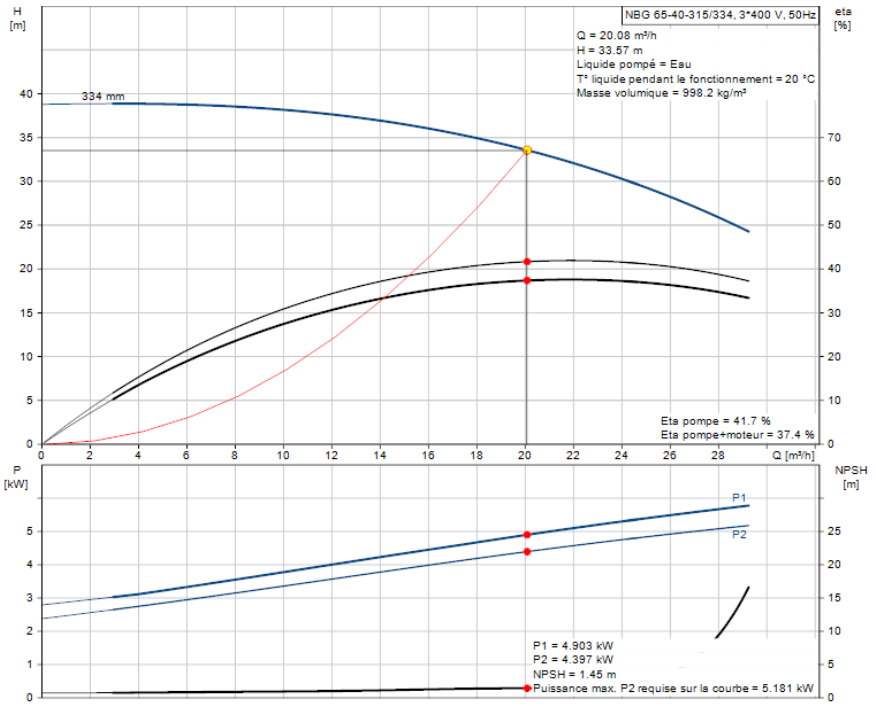


Figure 3. Grundfos performance curves

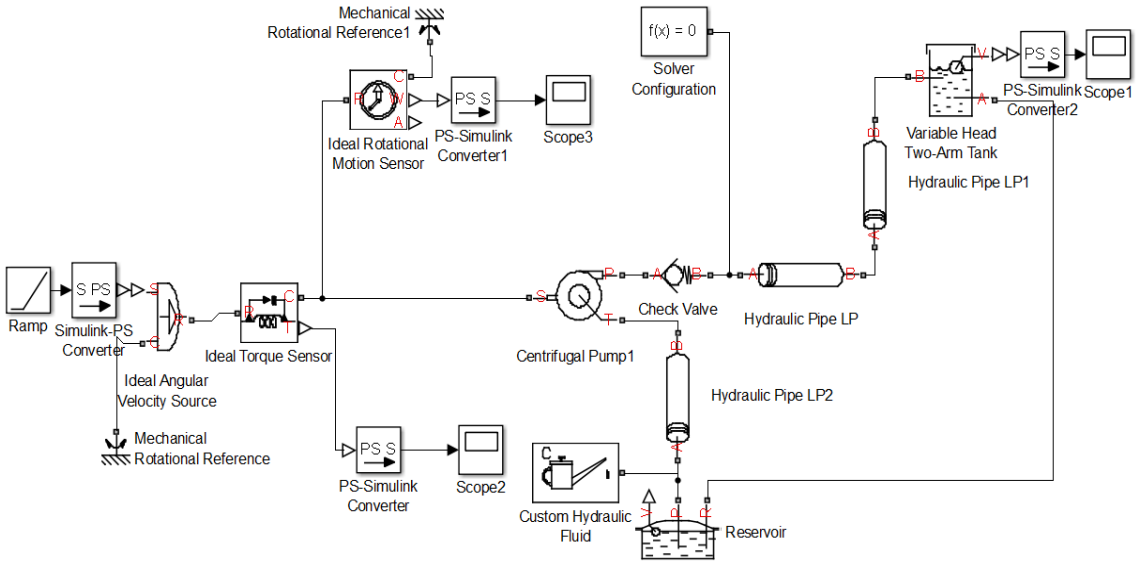


Figure 4. Centrifugal pump block diagram in Simscape

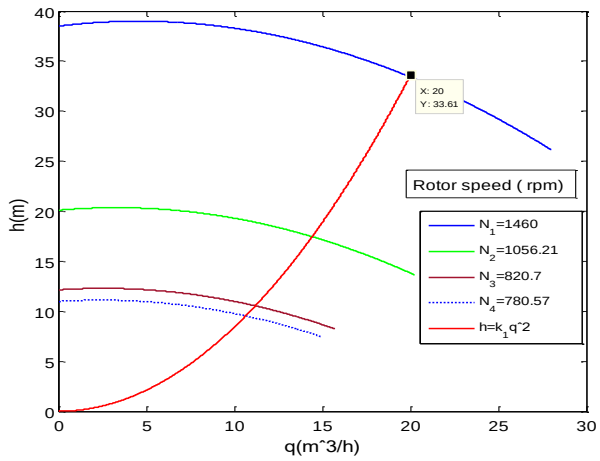


Figure 5. "Head-flow" characteristics of pump and pipeline

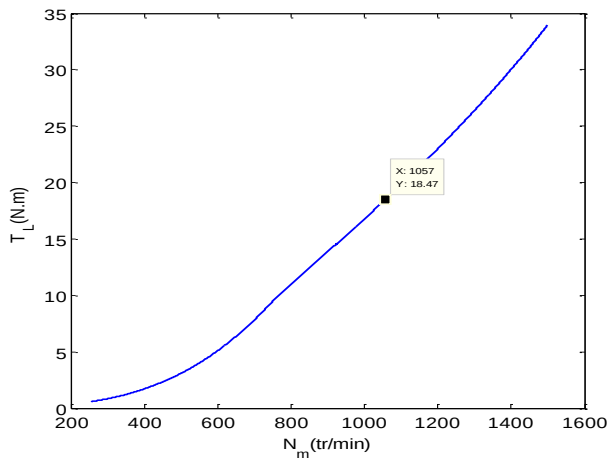


Figure 6. "Load torque-rotor speed" characteristic

## 3. ADAPTIVE CONTROLLER DESIGN

With the aim to achieve the MPP and to control the IM, the outputs to be controlled are expressed (18)-(21).

$$\lim_{t\to\infty} \varepsilon_1 = \lim_{t\to\infty} \frac{\partial P_{pv}}{\partial V_{pv}} = \lim_{t\to\infty}\left( I_{pv} + V_{pv}\frac{\partial I_{pv}}{\partial V_{pv}}\right) = 0 \tag{18}$$

$$\lim_{t\to\infty} \varepsilon_3 = \lim_{t\to\infty}\left(\omega_r(t) - \omega_{ref}(t)\right) = 0 \tag{19}$$

$$\lim_{t\to\infty} \varepsilon_4 = \lim_{t\to\infty}\left(\Psi_{rd}(t) - \Psi_{ref}\right) = 0 \tag{20}$$

Rotor speed reference is given by:

$$\omega_{ref}(t) = \sqrt[3]{\eta_{MP} V_{mpp} I_{mpp} / K} \tag{21}$$

where $\eta_{MP}$, $V_{mpp}$ and $I_{mpp}$ are the efficiency of the whole system, maximum voltage and maximum current of the PV generator respectively.

### 3.1. MPPT control law

Step 1: Let consider $\varepsilon_1$ as the MPP tracking error:

$$\varepsilon_1(t) = \frac{\partial P_{pv}}{\partial V_{pv}} = I_{pv} + V_{pv}\frac{\partial I_{pv}}{\partial V_{pv}} \tag{22}$$

The Lyapunov function and its derivative with respect to time can be defined as:

$$V_1 = \frac{1}{2}\varepsilon_1^2$$

$$\Rightarrow \dot{V}_1 = \varepsilon_1\dot{\varepsilon}_1 = \varepsilon_1\left(V_p\frac{\partial^2 I_{pv}}{\partial^2 V_{pv}} + 2\frac{\partial I_{pv}}{\partial V_{pv}}\right)\frac{dV_{pv}}{dt} = \varepsilon_1\left(\frac{I_{pv} - I_L}{C_p}\right) f \tag{23}$$

The virtual control law $\alpha_1$ and its derivative $\dot{\alpha}_1$ can be selected by forcing the Lyapunov function to be negative definite ($\dot{V}_1 = \varepsilon_1\dot{\varepsilon}_1 = -c_1\varepsilon_1^2 \le 0$ ) [7, 13].

$$\alpha_1 = (I_L)_d = I_{pv} + C_p c_1 \varepsilon_1 / f$$

$$\Rightarrow \dot{\alpha}_1 = \frac{\partial I_{pv}}{\partial V_{pv}}\dot{V}_{pv} + C_p\left(f c_1\dot{\varepsilon}_1 - c_1\dot{f}\varepsilon_1\right)/ f^2 \tag{24}$$

with:

$$\dot{f} = \dot{V}_{pv}(3h + \dot{h}) \quad ; \quad h = \frac{\partial^2 I_{pv}}{\partial^2 V_{pv}} \quad \Rightarrow \quad \dot{h} = V_{pv}\frac{\partial^3 I_{pv}}{\partial^3 V_{pv}} \tag{25}$$

and $c_1$ being a strictly positive constant parameter to be chosen.

Step 2: Let consider the tracking error between the actual virtual control and its desired value:

$$\varepsilon_2(t) = I_L - \alpha_1 \tag{26}$$

Let us define the second Lyapunov function and its derivative with respect to time:

$$V_2 = V_1 + \frac{1}{2}\varepsilon_2^2 \quad \Rightarrow \dot{V}_2 = -c_1\varepsilon_1^2 + \varepsilon_2(-\frac{f\varepsilon_1}{C_p} + \frac{V_{pv} - (1-u)V_b}{L_b}) \tag{27}$$

Duty cycle of DC-DC converter can be chosen in such way that the second Lyapunov function is negative definite:

$$u = \frac{L_b}{V_b}(\frac{f\varepsilon_1}{C_p} - c_2\varepsilon_2 + \dot{\alpha}_1) - \frac{V_{pv}}{V_b} + 1 \tag{28}$$

where $c_2$ is a constant parameter to be chosen.

### 3.2. Inverter control

Step 3: The tracking error between rotor speed and its reference and the error estimation of load torque can be expressed as:

$$\varepsilon_3 = \omega_r - \omega_{ref} \quad ; \tilde{a}_2 = a_2 - \hat{a}_2 \tag{29}$$

To guarantee stability and convergence, Lyapunov function is chosen positive and defined as:

$$V_3 = \frac{1}{2}\varepsilon_3^2$$

$$\Rightarrow \frac{dV_3}{dt} = \varepsilon_3(a_1\Psi_{rd}I_{sq} - \hat{a}_2 - a_3\omega_r - \frac{d\omega_{ref}}{dt}) - \tilde{a}_2\varepsilon_3$$

In this step, our objective is to select the control input which converges the origin $\varepsilon_3$ to 0. The control law is therefore given by (30):

$$I_{sq}^* = (-c_3\varepsilon_3 + \hat{a}_2 + a_3\omega_r + \frac{d\omega_{ref}}{dt}) / a_1\Psi_{rd} \tag{30}$$

where $c_3$ is a constant parameter to be designed.

Step 4: Let's consider the tracking error between rotor flux and its reference:

$$\varepsilon_4 = \Psi_{rd} - \Psi_{ref} \quad ; \tag{31}$$

The Lyapunov function and its derivative are defined (32).

$$V_4 = \frac{1}{2}\varepsilon_4^2 \quad \Rightarrow \frac{dV_4}{dt} = \varepsilon_4(\hat{a}_4 I_{sd} + \hat{a}_5\Psi_{rd}) \tag{32}$$

Direct stator current reference is expressed as:

$$I_{sd}^* = (-c_4\varepsilon_4 - \hat{a}_5\Psi_{rd}) / \hat{a}_4 \tag{33}$$

with $c_4$ being constant parameter to be designed.

### 3.3. Adaptive laws

Step 5: Let us consider a Lyapunov function and its derivative with repect to time:

$$V_5 = V_3 + \frac{\tilde{a}_2^{\,2}}{2\gamma_1} \Rightarrow \frac{dV_5}{dt} = \varepsilon_3\frac{d\varepsilon_3}{dt} + \frac{\tilde{a}_2}{\gamma_1}\frac{d\tilde{a}_2}{dt} \tag{34}$$

where $\gamma_1$ is constant parameter to be chosen.

Referring to step 3 and assuming that:

$$\hat{a}_2(t=0)=0 \quad ; \quad \varepsilon_3=\Psi_{rq}\neq 0 \quad ; \lim_{t\to\infty} I_{sq}=I_{sq}^{*} \tag{35}$$

The derivative of this Lyapunouv function becomes:

$$\frac{dV_5}{dt}=-c_1\varepsilon_3^2-\tilde{a}_2(\varepsilon_3+\frac{1}{\gamma_1}\frac{d\hat{a}_2}{dt}) \tag{36}$$

Using (35) and (30), and applying Laplace transformation, load torque estimator is chosen such that $\dot{V}_5$ is negative definite function [29].

$$\hat{a}_2(s)==\frac{a_1(\Psi_{rd}I_{sq}-\Psi_{rq}I_{sd})-a_3\omega_r-J\dfrac{d\omega_{ref}}{dt}}{1+\tau s} \tag{37}$$

The variation of rotor time-constant leads to the coupling between rotor flux and electromagnetic torque. Consequently, it is possible to deduce:

$$\hat{a}_5=a_{5n}+(\alpha+2\beta\Psi_{rq})\Psi_{rq}+\gamma\int(\Psi_{rq}+2\beta\Psi_{rq})\Psi_{rq}dt \tag{38}$$

where $\gamma$, $\alpha$, $\beta$, $a_{5n}$ and $\Psi_{rq}$ are respectively constant parameters to be chosen, the rated value of the inverse of rotor time constant and the quadrature component of rotor flux.

## 4. RESULTS AND DISCUSSION

To prove the excellent performance of the proposed controller and observers, we simulated the overall system in MATLAB/Simulink environment. The simulations are carried out at variable temperature and solar irradiance conditions. IM parameters are summarized in Table 3.

Table 3. IM parameters

| | |
|---|---|
| Rated power | 5.5 KW |
| Rated currents | 21/12 A |
| Efficiency of pump η | 41.70 % |
| Stator resistance $R_s$ | 2.25 Ω |
| Rotor resistance $R_r$ | 0.7 Ω |
| Stator inductance $L_s$ | 0.1232 H |
| Rotor inductance $L_r$ | 0.1122 H |
| Mutual inductance *M* | 0.1118 H |
| Leakage coefficient σ | 0.09 |
| Moment of inertia J | 0.038 $Kgm^2$ |
| Viscous friction coefficient F | 0.0124 $Kgm^2$ |

The sudden variations in the solar irradiance from 1000 to 500 $W/m^2$ and the temperature from 25 °C to 50 °C as a function of time are considered. The reference value of the rotor flux is kept at its nominal value (1 Wb) while the mechanical speed reference is calculated referring to the optimal power. The rotor flux estimator is based on the sliding mode control [29]. This estimator requires knowledge of the stator resistance. To prove the robustness of the controller to the stator resistance variation, we programmed a slow variation of this resistance from 2.5 Ω (nominal value) to 3.3 Ω (32 percent variation).

Based on the simulation results, Figure 7 shows the controller reaches the MPP coordinates summarized in Table 1. In addition, the response of the mechanical speed obtained by the same controller tracks accurately its reference value. It is clearly obvious that the decoupling is achieved during the operation of the system and the quadrature component of the rotor flux varies only during the response time of the rotor time-constant observer.

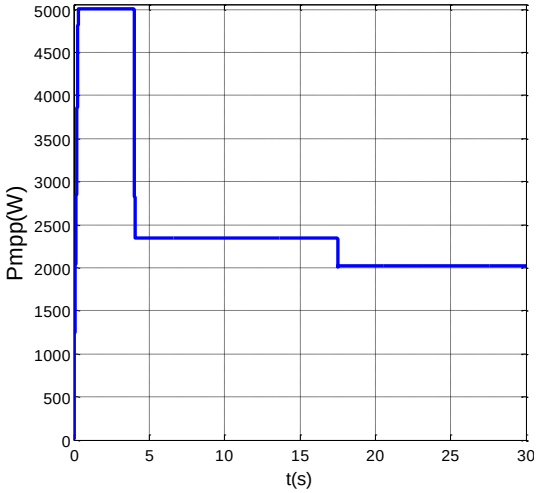


Figure 7. Maximum power of PV generator

The actual rotor time constant of the machine and the observed load torque imposed by the centrifugal pump, calculated by the expressions developed above (37 and 38) are used to adapt the rotor time-constant, to eliminate the use of an expensive mechanical sensor and to avoid the use of complex models of this pump in the indirect vector control law. Therefore, the calculation of the reference synchronous speed uses this estimated rotor time-constant which corresponds to the real conditions of the machine. Parameters of the controller are given (39).

$$c_1 = 1e3\,; c_2 = 1e5\,; c_3 = 1e3; c_4 = 1e5; \alpha = 40; \beta = 60; \gamma = 0.1; \tau = 0.2s \qquad (39)$$

The simulation results for these tests are shown in Figure 8 to Figure 15. It is quite remarkable from these figures that the adaptation of the rotor time-constant and of the load torque are accomplished whatever are the variations applied to the rotor and stator resistances of the machine and the variations in climatic conditions. In addition, these two observers are robust against the variations of stator resistance and optimal power. These responses do not exceed their desired values, require only measurable or estimated induction machine state variables and the obtained results are very satisfactory. Load torque observer is independent of the centrifugal pump variables and parameters. Unlike the controllers presented in reference [13], the use of anti-saturation function can eliminate the excessive currents at transient state of current controlled induction motor.

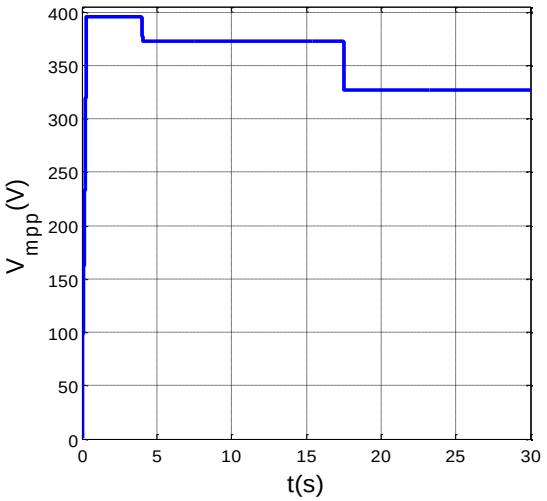


Figure 8. Maximum voltage of PV generator

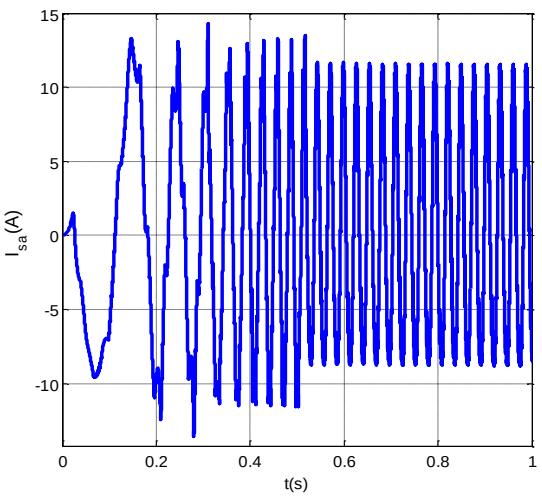


Figure 9. Stator current

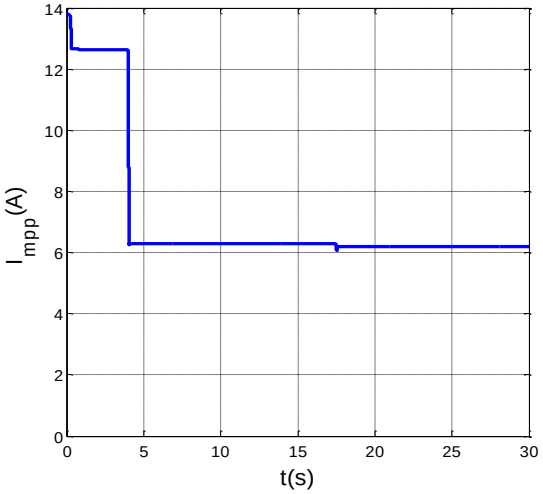


Figure 10. Maximum current of PV generator

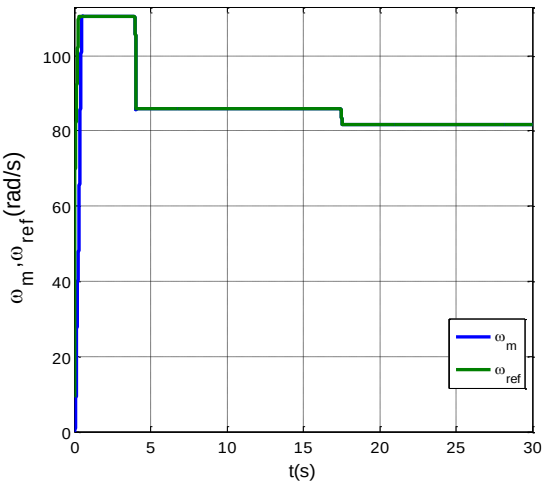


Figure 11. Rotor speed

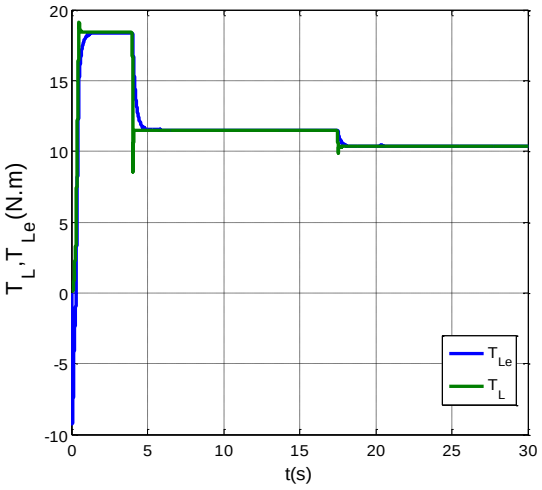


Figure 12. Load torque

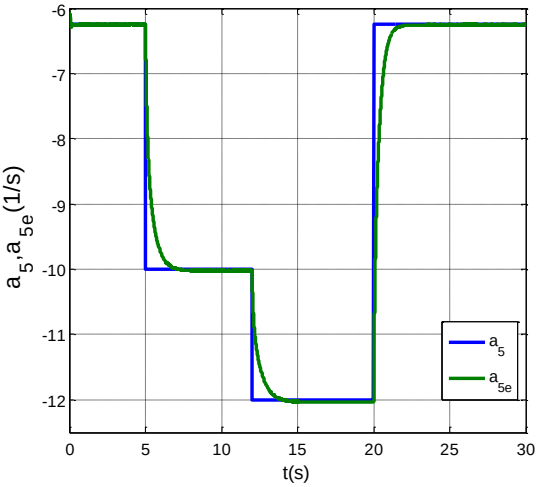


Figure 13. Rotor time constant

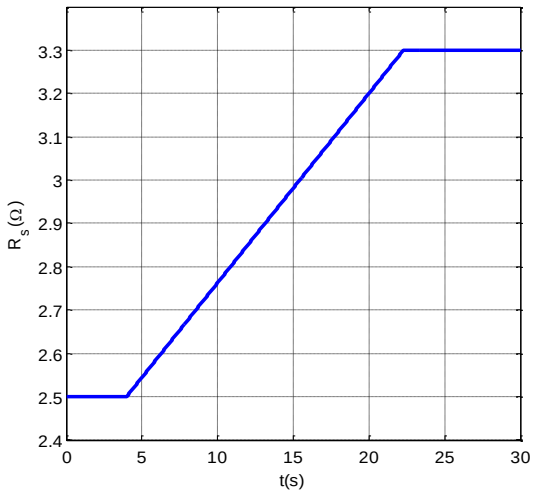


Figure 14. Stator resistance

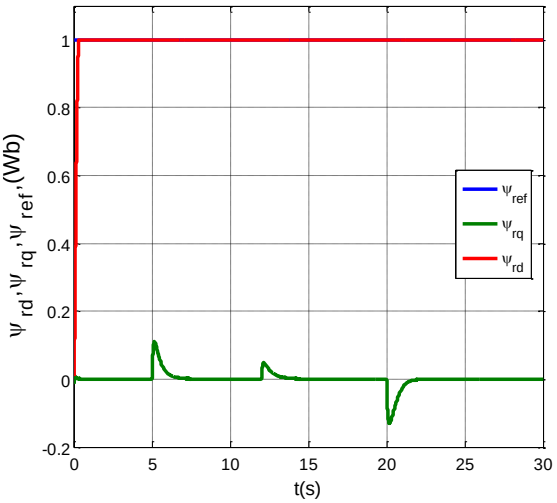


Figure 15. Rotor flux estimator

## 5. CONCLUSION

This paper presented the design and simulation of an adaptive vector control of the induction motor, driving a centrifugal pump, and supplied by a photovoltaic generator. This adaptive controller was introduced to online estimate rotor time constant variation in order to achieve the decoupling between rotor flux and electromagnetic torque and to avoid the use of mathematical model of the centrifugal pump in control laws. To optimize the control and adaptive laws, this controller is combined with indirect rotor field oriented control and the induction machine is fed by a current controlled voltage source inverter (CC-VSI). It can be seen from simulation results that the controller tracked accurately the MPP coordinates and the rotor speed reference. The proposed observers showed good results in the estimation of the rotor time-constant and the load torque disturbance and in the adaptation of these variables in an indirect vector control of the induction motor under abrupt climatic condition variations. In addition, these observers permitted achieving the decoupling between the rotor flux and the electromagnetic torque and their performances are very satisfactory. The control and adaptation laws were based only on the equations of the induction machine and had a slow dynamic response exhibiting the behavior of a first order system. The use of an anti-saturation function permitted to limit high current overshoot in transient state. Even if the adaptive laws were used in highly nonlinear applications, the robustness and the stability of the whole system were guaranteed and validated that these obtained performances will enable us to use them in real implementation.

## REFERENCES


[1] IRENA, "Renewable Capacity Statistics 2020," *International Renewable Energy Agency (IRENA)*, Abu Dhabi, 2020.

[2] A. Alhamwi1, D. Kleinhans, S. Weitemeyer and T. Vogt, "Moroccan National Energy Strategy Reviewed from a Meteorological Perspective," *Energy Strategy Reviews*, vol. 6, pp. 39-47, 2015.

[3] S. Odeh and M. Behnia, "Improving Photovoltaic Module Efficiency Using Water Cooling," *Heat Transfer Engineering*, vol. 30, no. 6, pp. 499-505, 2009.

[4] J. C. Joshi and D. P. Kothari, "Performance analysis of a directly coupled photovoltaic water-pumping system," *IEEE Transactions on Energy Conversion*, vol. 19, no. 3, pp. 613-618, 2004.

[5] T. Esram and P. L. Chapman, "Comparison of photovoltaic array maximum power point tracking techniques," *IEEE Transactions on Energy Conversion*, vol. 22, no. 2, pp. 439-449, 2007.

[6] R. Alik, A. Jusoh and T. Sutikno, "A Study of Shading Effect on Photovoltaic Modules with Proposed P&O Checking Algorithm," *International Journal of Electrical and Computer Engineering (IJECE)*, vol. 7, no. 1, pp. 29-40, 2017.

[7] M. El Malah, A. Ba-razzouk, M. Guisser, E. Abdelmounim and M. Madark, "Backstepping based power control of a three-phase single-stage grid-connected PV system," *International Journal of Electrical and Computer Engineering (IJECE)*, vol. 9, no. 6, pp. 4738-4748, 2019.

[8] H. Bahri, M. Aboulfatah, M. Guisser, E. Abdelmounim and M. El Malah, "Integral Backstepping Control for Maximum Power Point Tracking and Unity Power Factor of a Three Phase Grid Connected Photovoltaic System," *International Journal of Electrical and Computer Engineering (IJECE)*, vol. 7 no. 4, pp. 1671-1680, 2017.

[9] K. Zhang, P. Cheng and L. He, "A maximum power point tracking method combined with constant voltage tracking & variable step-size perturbation," *Sensors & Transducers*, vol. 175, no. 7, pp. 150-155, 2014.

[10] M. Madark, A. Ba-razzouk, E. Abdelmounim and M. El Malah, "Linear and nonlinear controllers of a solar photovoltaic water pumping system," *Bulletin of Electrical Engineering and Informatics*, vol. 9, no. 5, pp. 1861-1872, 2020.

[11] M. Guisser, A. El-Jouni, M. Aboulfatah and E. Abdelmounim, "Nonlinear MPPT Controller for Photovoltaic Pumping System Based on Robust Integral Backstepping Approach," *International Review on Modelling and Simulations*, vol. 7, no. 3, pp. 481-488, 2014.

[12] V.T. Akhila and S. Arun, "Review of Solar PV Powered Water Pumping System Using Induction Motor Drive," *IOP Conf. Series: Materials Science and Engineering*, vol. 396, no. 1, 2018, Art. no. 012047.

[13] M. Madark, A. Ba-Razzouk, E. Abdelmounim and M. El Malah, "A New Induction Motor Adaptive Robust Vector Control based on Backstepping," *International Journal of Electrical and Computer Engineering (IJECE)*, vol. 7, no. 3, pp. 1983-1993, 2017.

[14] V. Vongmanee and V. U. Monyakul, "Vector Control of Induction Motor Drive System Supplied by Photovoltaic Arrays," *IEEE 2002 International Conference on Communications, Circuits and Systems and West Sino Expositions*, vol. 2, Chengdu, China, 2002, pp. 1753-1756.

[15] N. Benbaha, F. Zidani, M. Nait Said, S. Boukebbous, H. Ammar, "Optimal energy control of induction motor standalone photovoltaic-battery pumping system," *2017 6th International Conference on Systems and Control (ICSC)*, Batna, 2017, pp. 622-628.

[16] M. Arrouf and S. Ghabrour, "Modelling and simulation of a pumping system fed by photovoltaic generator within the MATLAB/Simulink programming environment," *Desalination*, vol. 209, no. 1-3, pp. 23-30, 2007.

[17] V. L. Streeter and E. B. Wylie, "Fluid Mechanics," *Eighth Edition, McGraw-Hill, Inc*., New York, 1985.

[18] W. Z. Fam and P. Goswami, "Simulation and Testing of a Photovoltaic Solar-Powered Water Pumping Systems," *Energy Sources*, vol. 14, no. 3, pp. 265-272, 1992.

[19] J. H. Eckstein, T. Townsend, W. A. Beckman and J. A. Duffie, "Photovoltaic Powered Energy Systems," *Proceedings of the ASES Solar 90 Conference*, Austin TX, 2020.

[20] S. Shukla and B. Singh, "An Effective Solar PV Fed Modified Vector Control of IMD for Water Pumping," *2017 14th IEEE India Council International Conference (INDICON)*, Roorkee, 2017, pp. 1-6.
[21] A. El Fadili, F. Cuny, A. El Magri, M. Stitou, F. Giri, J. M. Janik and F. Z. Chaoui, "Backstepping Control of Photovoltaic-Grid Hybrid Power Feed Water Pump," *IFAC-PapersOnLine*, vol. 50, no. 1, pp. 6540-6545, 2017.
[22] Geet Jain, Arun Shankar V. K. and Umashankar S., "Modelling and Simulation of Solar Photovoltaic fed Induction Motor for Water Pumping Application using Perturb and Observer MPPT Algorithm," *2016 International Conference on Energy Efficient Technologies for Sustainability (ICEETS)*, Nagercoil, India, 2016, pp. 250-254.
[23] M. Madark, A. Ba-Razzouk, E. Abdelmounim and M. El Malah, "Adaptive Vector Control of Induction Motor Using CTMVC," *International Review on Modelling and Simulations (IREMOS)*, vol. 10, no. 4, pp. 303-312, 2017.
[24] E. Can, "Novel high multilevel inverters investigated on simulation," *Electrical Engineering*, vol. 99, no. 2, pp. 633-638, 2017.
[25] Can, E., "A new multi-level inverter with reverse connected dual dc to dc converter at simulation," *International Journal of Modelling and Simulation*, pp. 1-13, 2020, doi: 10.1080/02286203.2020.1824451.
[26] T. G. Hicks and T. W. Edwards, "Pump Application Engineering," *McGraw-Hill*, NY, 1971
[27] I. J. Karassic, J. P. Messina, P. Cooper and C. C. Heald, "Pump Handbook," *Third edition, McGraw-Hill*, NY, 2001.
[28] F. White, "Fluid Mechanics," *Third Edition, McGraw-Hill*, Inc., New York, 1994.
[29] M. Madark, A. Ba-Razzouk, E. Abdelmounim and M. El Malah, "An Effective Method for Rotor Time-Constant and Load Torque Estimation for High Performance Induction Motor Vector Control," *International Review on Modelling and Simulations (IREMOS)*, vol. 10, no. 6, pp. 410-422, 2017.